Strain relaxation and superconductivity in electron-doped $Sr_{0.85}La_{0.15}CuO_2$ thin films grown by laser ablation

Victor Leca[1,2], Jochen Tomaschko[2], Mihai Danila[1], Di Wang[3], Wim A. Bik[4], Reinhold Kleiner[2], and Dieter Kölle[2]

[1]National Institute for Research and Development in Microtechnologies, Bucharest, Romania
[2]Center for Collective Quantum Phenomena in LISA+, University of Tübingen, Germany
[3]Karlsruhe Institute for Technology, Institute for Nanotechnology, Karlsruhe, Germany
[4]AccTec BV, TN/Cyclotrongebouw, Technical University of Eindhoven, The Netherlands

Outline

Motivation behind this work

$Sr_{1-x}La_xCuO_2$ (x=0.15) thin films:

- - Pulsed Laser Deposition growth by the reduction method on different substrates ($SrTiO_3$/$BaTiO_3$, $KTaO_3$, and $DyScO_3$);
- - microstructural studies and epitaxial strain evolution;
- - short overview of the results on the superconducting order parameter symmetry studies.

Conclusions

Motivation of the work

1. Symmetry of the superconducting order parameter in the electron-doped $Sr_{1-x}La_xCuO_2$ compounds (SLCO, x=0.10-0.175) from:

i. phase sensitive tunneling experiments based on 0/π-SQUIDs (on $SrTiO_3$ tetracrystals)

Tomaschko et al., PRB 86, 094509 (2012)

ii. tunneling studies across Josephson contacts between SLCO and a low-T_c superconductors (Nb), with known s-wave symmetry

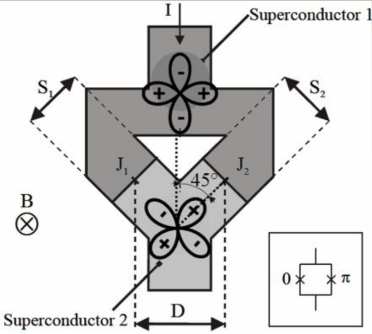

2. Studies on SLCO Josephson junctions:

i. grain-boundary junctions based on c-axis oriented SLCO films

Tomaschko et al., PRB 84, 0214507 (2011)

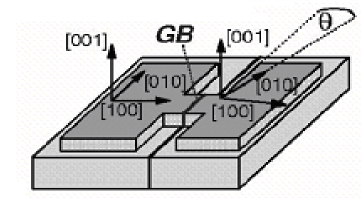

ii. ramp type SLCO/Me/Nb (Me=Ag, Au) junctions

iii. planar c-axis SLCO/Au/Nb tunnel junctions

Tomaschko et al., PRB 84, 064521 (2011)

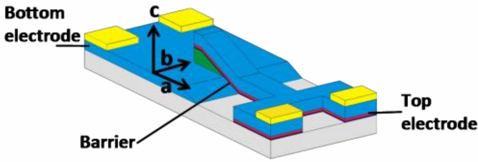

3. Better understanding of the correlation between strain, microstructure, and electrical transport properties in SLCO thin films grown by PLD on different substrates ($SrTiO_3$, $KTaO_3$, and $DyScO_3$)

Leca et al., APL 89, 92504 (2006); Appl. Phys. A 93, 779 (2008)

Tomaschko et al., PRB 85, 024519 (2012)

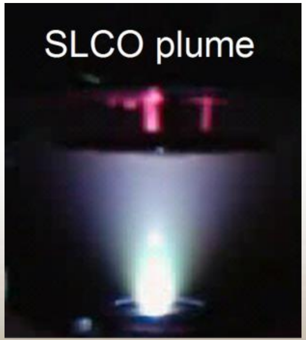

The $Sr_{1-x}La_xCuO_2$ compounds

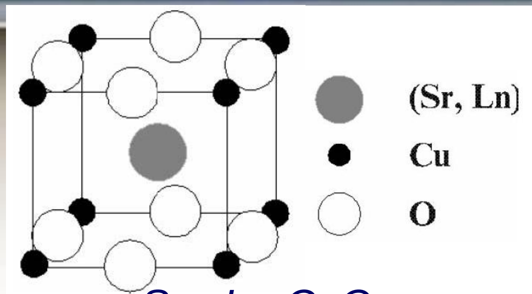

$Sr_{1-x}Ln_xCuO_2$
-infinite-layer (IL) type structure
- $T_{c,max}$ = 43 K

Smith et al., Nature 351 (1991)
Adachi et al., Physica C 196 (1992)

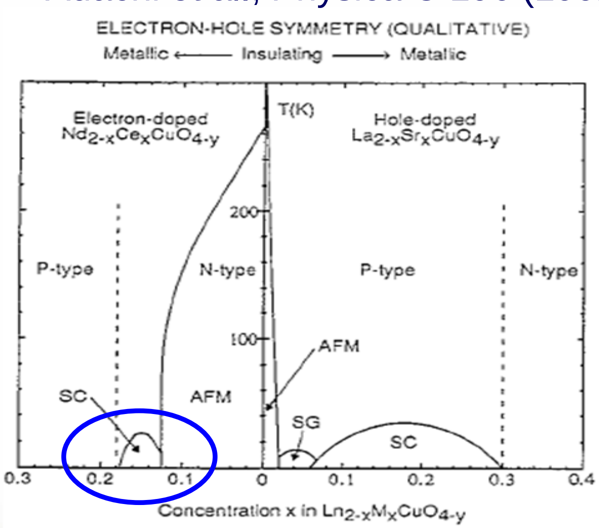

Phase diagram for T'-$Ln_{2-x}Me_xCuO_4$

Armitage et al., RMP 82 (2010)

Thin films by the reduction method

(MBE growth on (001) $KTaO_3$)

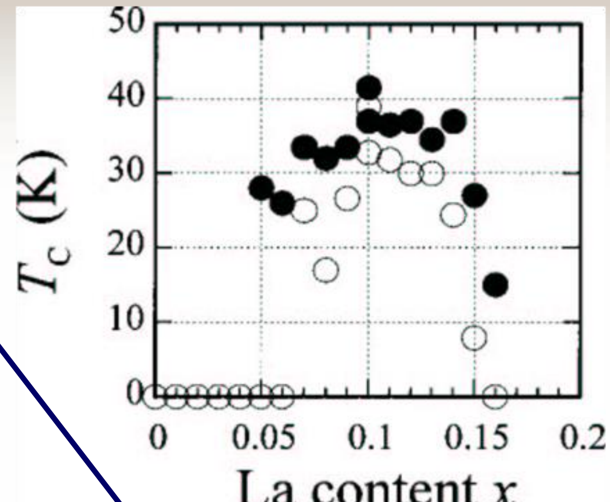

1st thin film single crystals with T_c ~ 42 K

Bulk synthesis:
high P (~ GPa),
high T (1000°C)

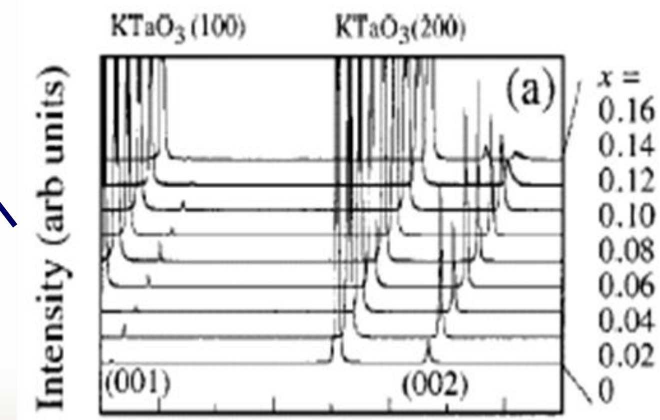

Secondary phase forms for x> 0.12

Unknown phase diagram for IL phases

Karimoto et al., APL 79 (2001)

The $Sr_{1-x}La_xCuO_2$ compounds

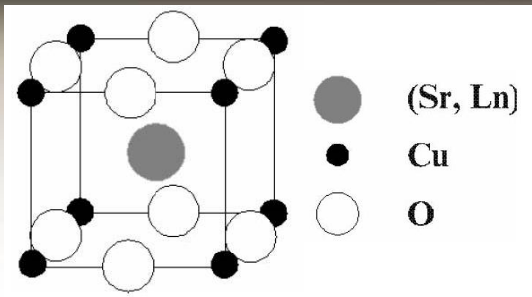

$Sr_{1-x}Ln_xCuO_2$ structure)

Thin films by the oxidation method

(PLD growth on (001) $KTaO_3$)

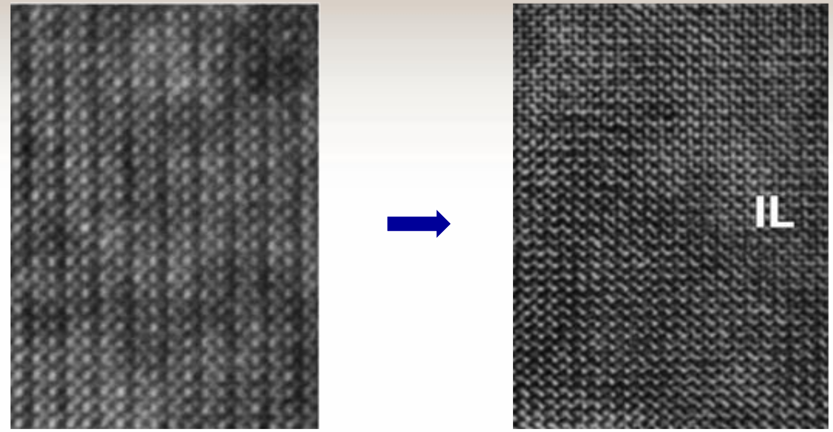

Starting phase:
$2\sqrt{2}a_p \times 2\sqrt{2}a_p \times c$ (super)structure

End phase:
infinite layer type structure

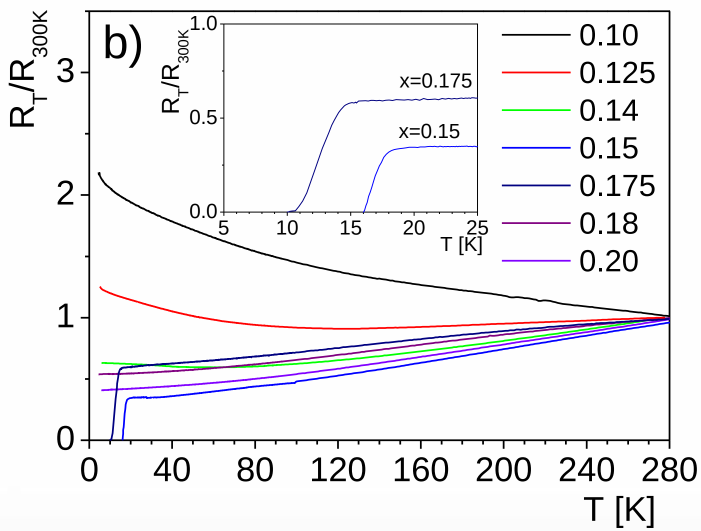

Evolution of T_c with La doping

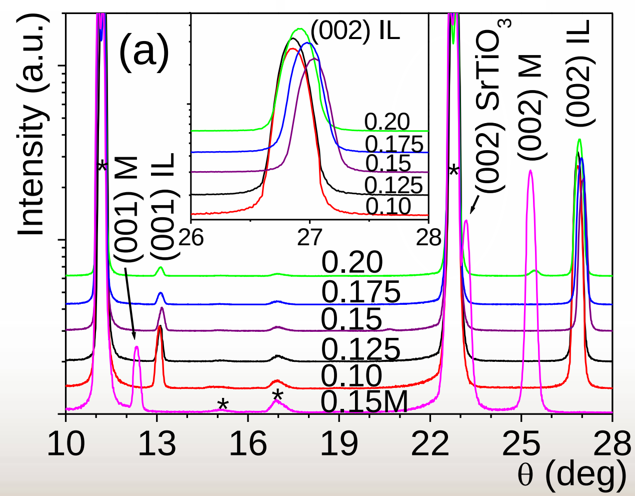

Low O_2 pressure required during growth

Evolution of composition with La doping

Increased phase stability up to 20 % La; superconductivity for x=0.15-0.175.

Leca et al., APL 89 (2006)

Requirements for $Sr_{1-x}La_xCuO_2$-based junctions

Grain-boundary

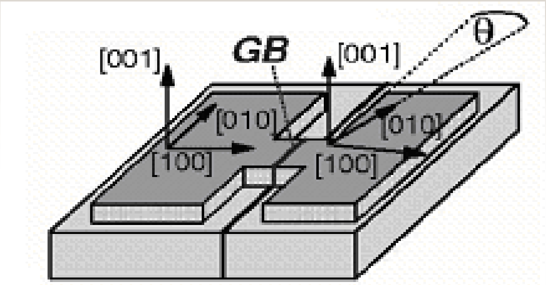

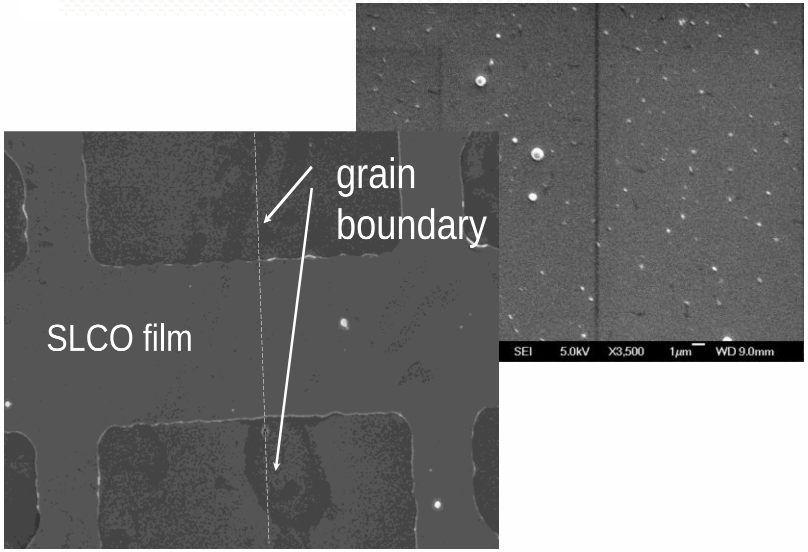

Single phase, c-axis oriented films required

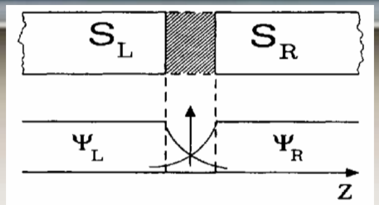

Josephson junction
(schematic representation)

Ramp-type and planar
(SrLaCuO/Au/Nb)

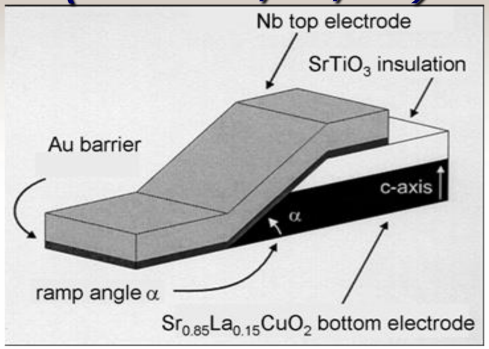

AFM of a ramp-type junction

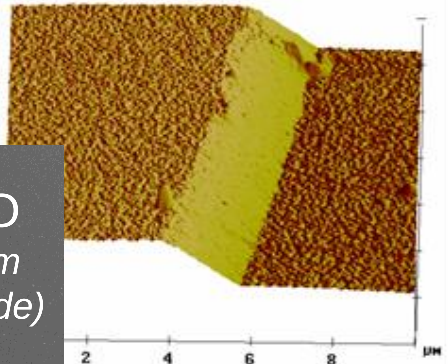

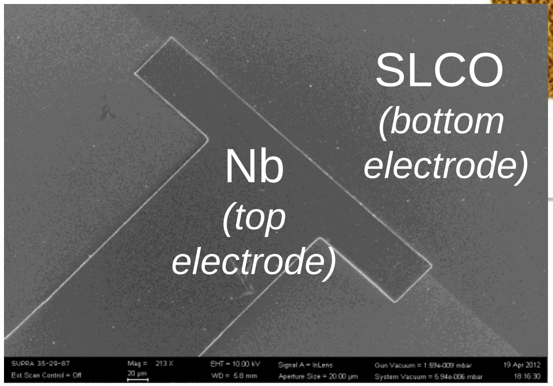

SEM of a 200 μm wide junction

Single phase, c-axis oriented SLCO films, with smooth surface and sharp oxide-metal interface required

$Sr_{1-x}La_xCuO_2$ ($x \approx 0.15$) growth parameters

On (001) $KTaO_3$ and (110) $DyScO_3$

$Sr_{1-x}La_xCuO_2$ (SLCO):

T_d = 500-575 ^oC
P_d = 0.20-0.40 mbar O_2
Post-deposition vacuum annealing (reduction) at T_d and 10^{-7} mbar:
- 10-20 min ($KTaO_3$ case)
- 20-30 min ($DyScO_3$ case)

T_c: up to 24 K, on $KTaO_3$
up to 18 K, on $DyScO_3$

Film's composition (x_t=0.15 target), from RBS data:
- x_f = 0.145, film grown on $KTaO_3$
- x_f = 0.135, film grown on $DyScO_3$

a_{KTO}=3.989 Å, a_{SLCO}~3.985 Å
$a_{DSO(110)}$=3.944 Å, a_{SLCO}~3.955 Å

On $BaTiO_3$- buffered (001) $SrTiO_3$

$BaTiO_3$ (BTO):

T_d = 700-850 ^oC
P_d = 0.10 mbar O_2
Post-deposition annealing:
-15 min @ 950^{o}C, under 0.10 mbar O_2, and 30 min @ 950^{o}C, in vacuum (10^{-7} mbar)

$Sr_{1-x}La_xCuO_2$ (SLCO):

T_d = 550-600 ^oC
P_d = 0.20 mbar O_2
Post-deposition annealing (reduction):
45-60 min @ 550 ^oC, in vacuum (10^{-7} mbar)

T_c: up to 21 K

Film's composition (x_t = 0.15 target), from RBS data: x_f = 0.145

a_{STO}=3.905 Å, a_{BTO}~3.990 Å, a_{SLCO}~3.967 Å

Tomaschko, Leca, Selistrovski, Diebold, Jochum, Kleiner, Koelle, Phys. Rev. B 85 (2012)

$Sr_{1-x}La_xCuO_2$ ($x \approx 0.15$) grown on $BaTiO_3/SrTiO_3$ (001)

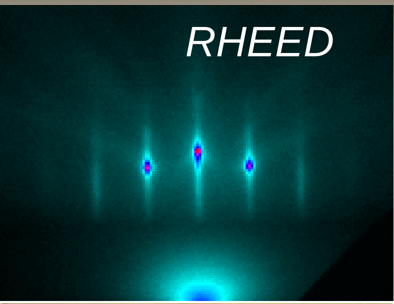

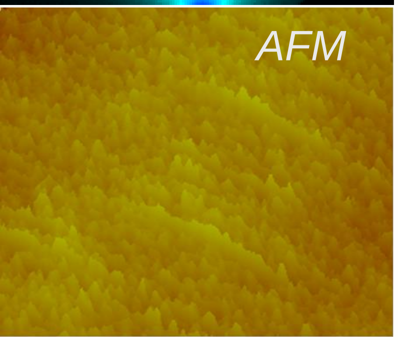

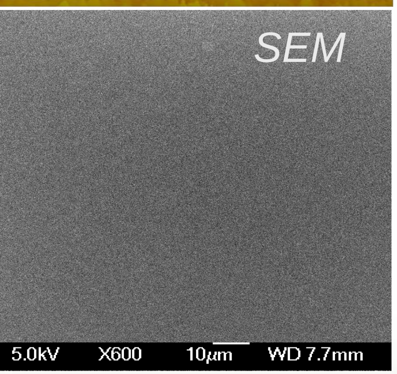

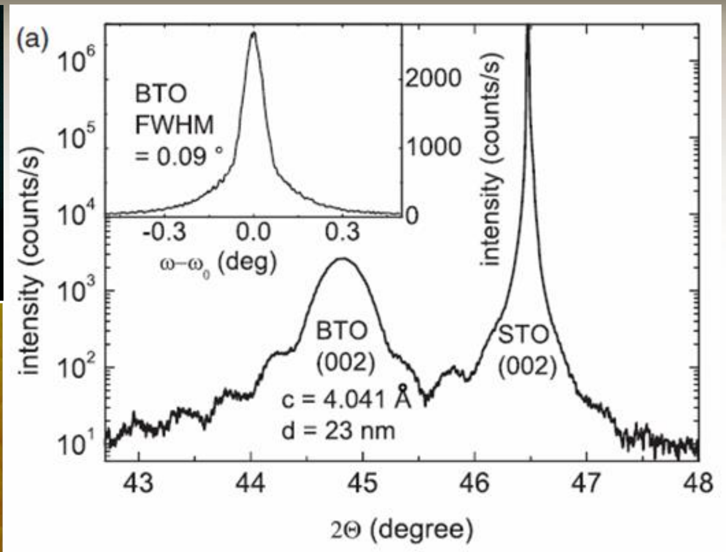

XRD 2θ/ω and rocking curve scans of BTO/STO symmetric (002) reflection; film thickness estimated from Laue fringes

The $BaTiO_3$ buffer layer

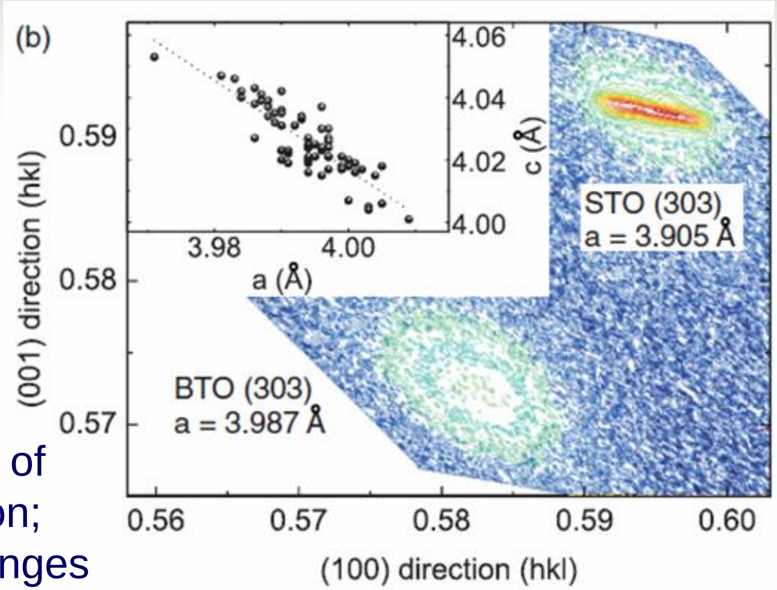

XRD rsm around asymmetric (303) Bragg reflection of BTO/STO

Tetragonal symmetry

Deposition conditions for $BaTiO_3$:

T_d=750°C, P_d=0.10 mbar O_2, E_d=1.75 J/cm²;
annealing 15 min/950°C/0.10 mbar O_2 and 30 min/950°C/10^{-7} mbar

Tomaschko et al., Phys. Rev. B 85 (2012)

$Sr_{1-x}La_xCuO_2$ ($x \approx 0.15$) grown on $BaTiO_3/SrTiO_3$ (001)

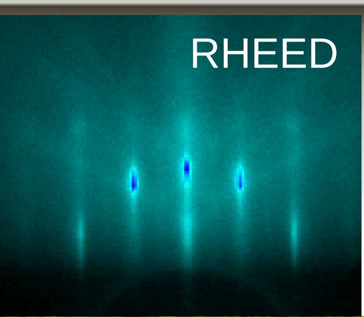

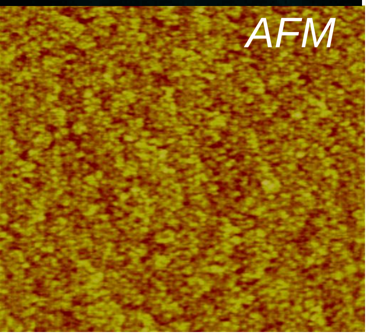

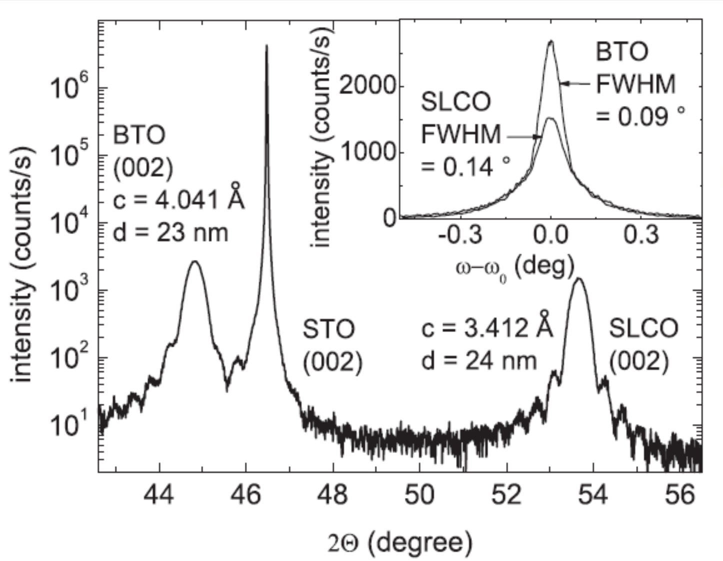

XRD 2θ/ω and rocking curve scans of (002) reflections

The $Sr_{1-x}La_xCuO_2$ films

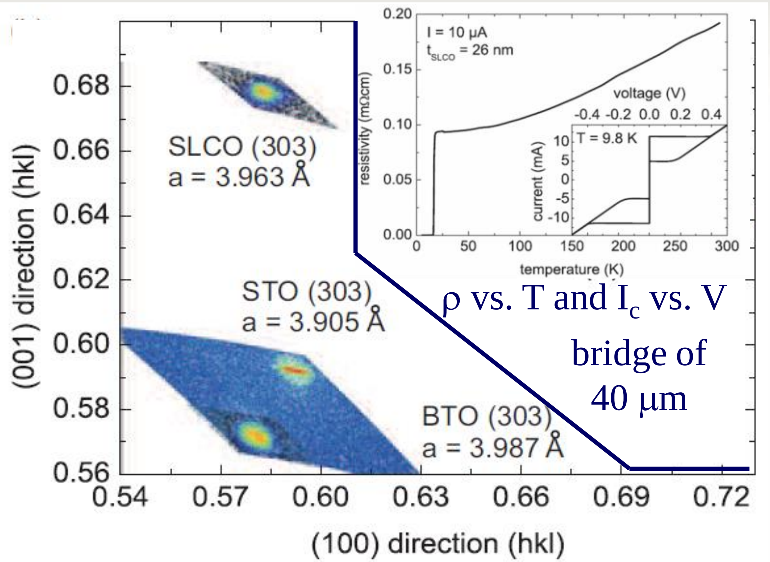

XRD rsm of (303) SLCO/BTO/STO

No presence of secondary phase; tetragonal, IL-type structure; preferential orientation (c-axis)

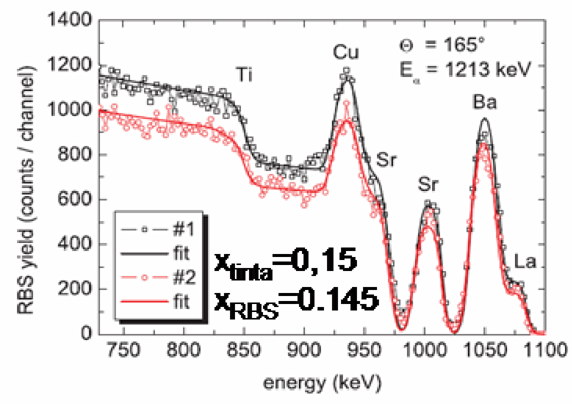

RBS data

Deposition conditions for $Sr_{1-x}La_xCuO_2$:

T_d=550ºC, 0.30 mbar O_2; annealing 50 min/550ºC/10^{-7} mbar

$T_{c,0}$=10-21 K; $J_{c@4.2K}$=2.1×10^6 A/cm^2

Tomaschko et al., Phys. Rev. B 85 (2012)

$Sr_{1-x}La_xCuO_2$ (x≈0.15) grown on $BaTiO_3/SrTiO_3$ (001)

Microstructure

HRXRD

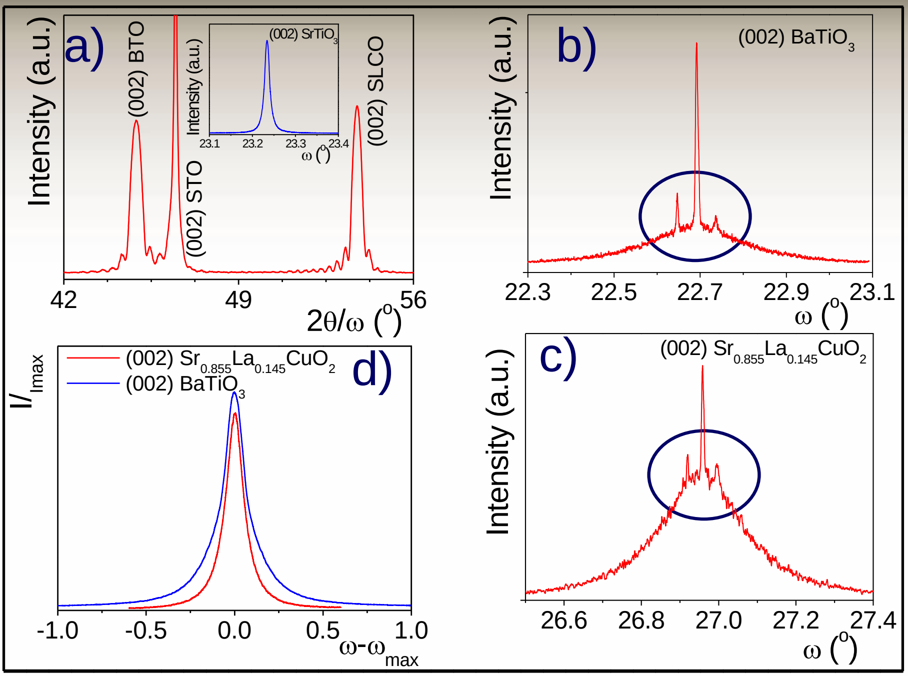

HRXRD (a-c) and XRD (d) data for a BTO/SLCO film with d_{BTO}=35 nm

Misfit strain accommodation by lattice modulations

Two components in ω scans: strained and relaxed

Buffer layer thickness dependent microstructure:
- lattice modulations visible ***only*** in the HRXRD scans and for d_{BTO} > 30 nm

HRXRD: triple axes configuration
XRD: double axes configuration

HRTEM

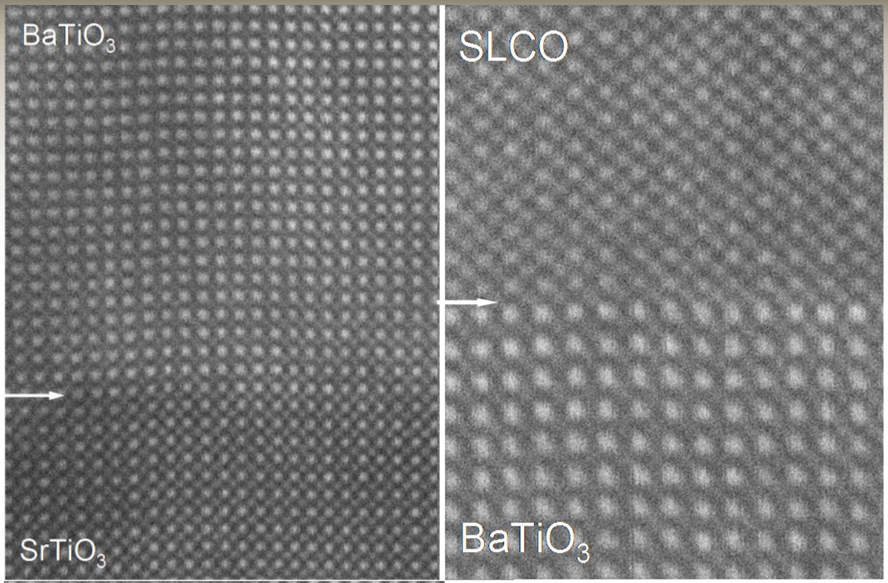

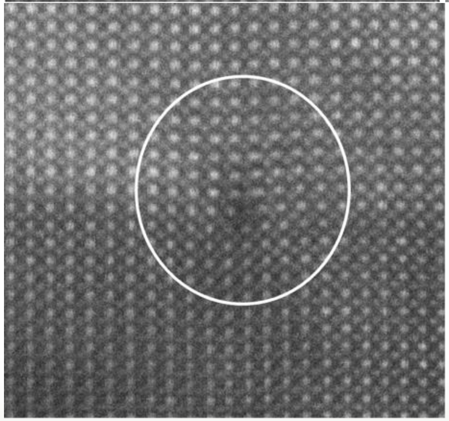

edge dislocation at the STO/BTO interface

Migration of the structural defects at the BTO/STO interface due to high temperature annealing

Terai et al., APL 80 (2002)

$Sr_{1-x}La_xCuO_2$ (x≈0.15) grown on $KTaO_3$ (001)

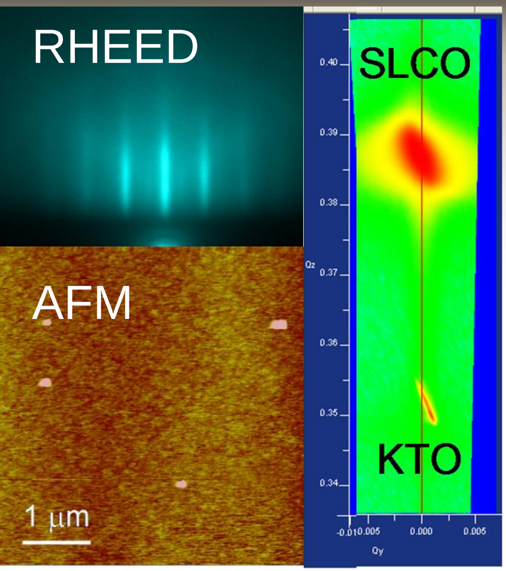

RHEED, AFM, and XRD rsm of (101) plane

XRD data

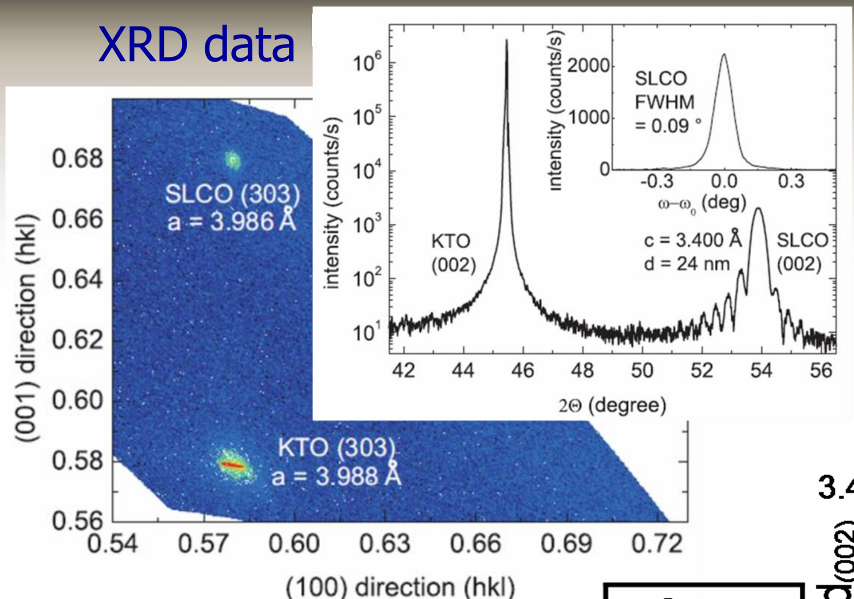

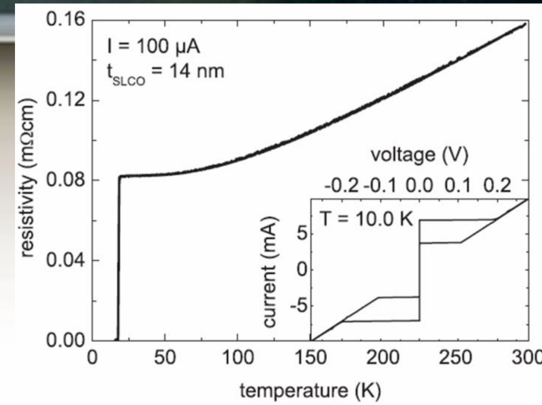

R vs. T and I_c vs. V

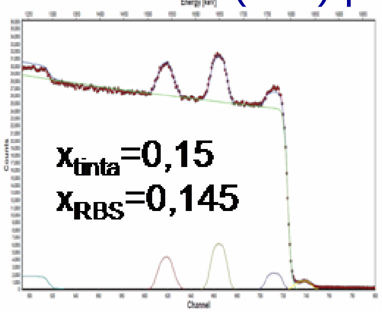

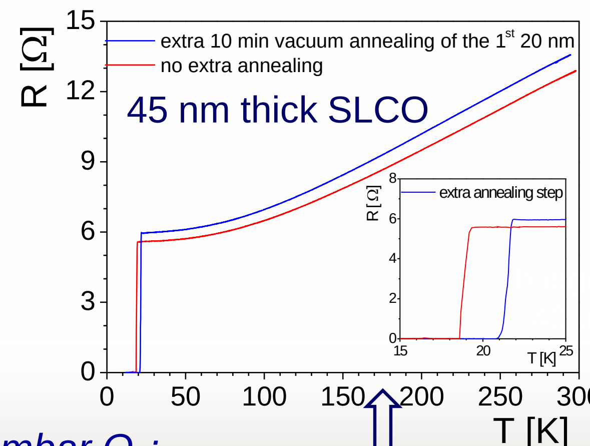

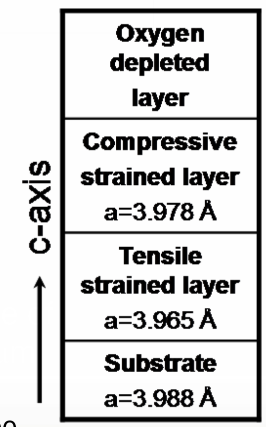

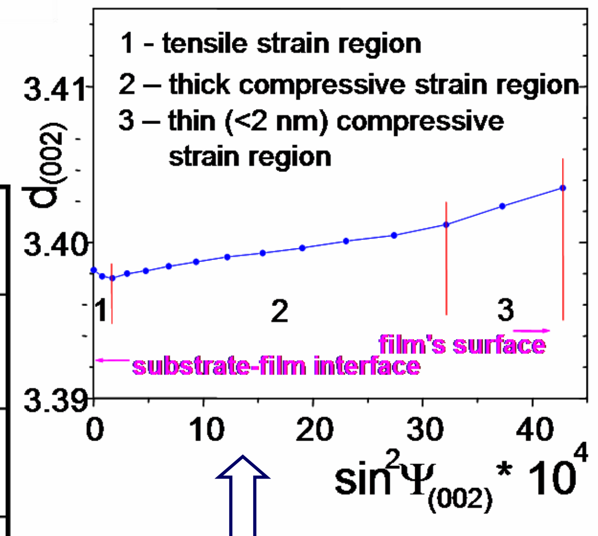

Deposition conditions:

T_d=550°C, P_d=0.20-0.40 mbar O_2;
annealing 10-20 min/550°C/10^{-7} mbar
$T_{c,0}$=12-24 K, $J_{c@4.2K}$=2.1×10^6 A/cm^2

Two steps annealing:
T_c evolution

In-plane strain evolution: tensile strain region at the substrate-film interface

Tomaschko et al., Phys. Rev. B 85 (2012)

$Sr_{1-x}La_xCuO_2$ ($x \approx 0.15$) grown on $DyScO_3$ (110)

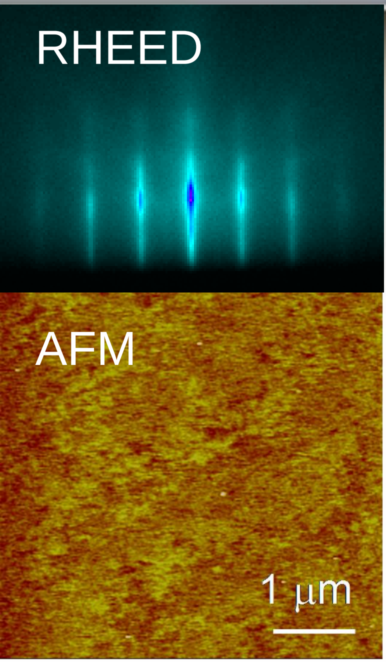

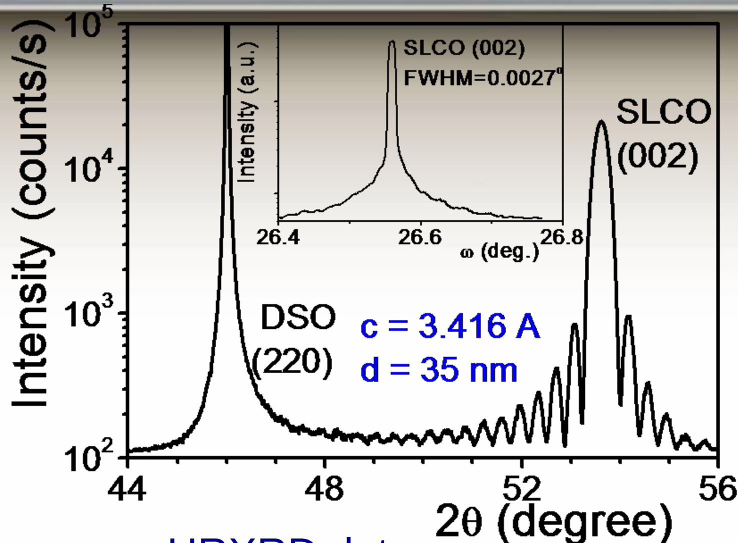

HRXRD data

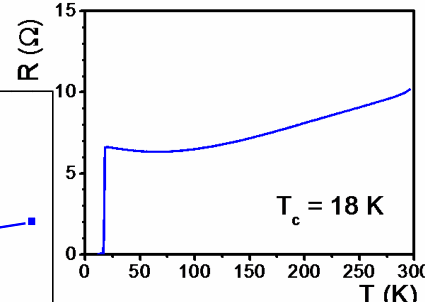

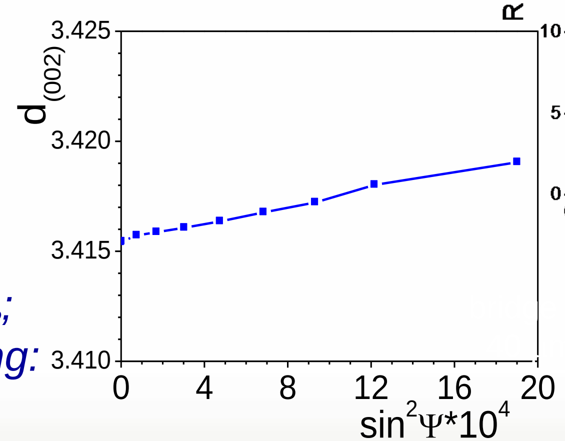

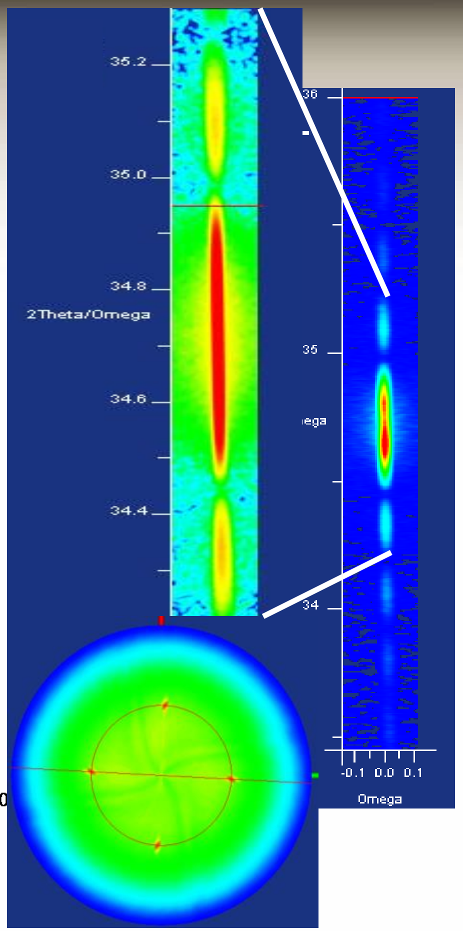

Deposition conditions:

T_d=550°C, 0.20 mbar O_2;
Post deposition annealing:
25 min/550°C/10^{-7} mbar
$T_{c,0}$=12-18 K

Strain evolution:
in-plane compressive strain

- No interface tensile strain layer

R vs. T evolution

HRXRD rsm and pole figure of asymmetric (101) plane
Presence of Laue fringes indicates high crystalinity

HRTEM results on $Sr_{1-x}La_xCuO_2$ ($x \approx 0.15$) film

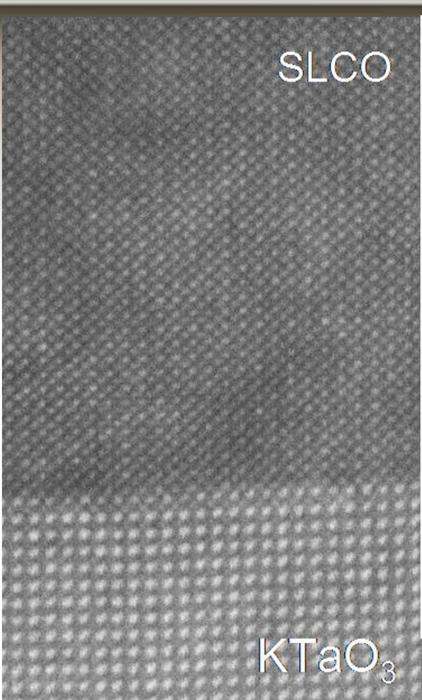

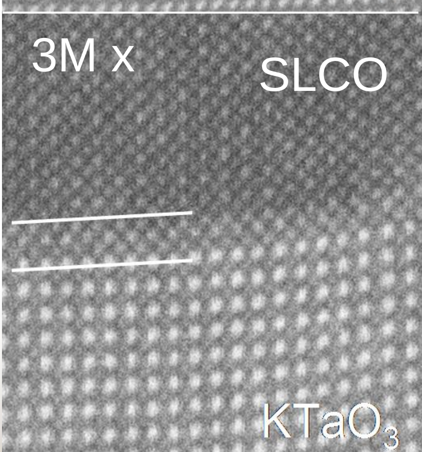

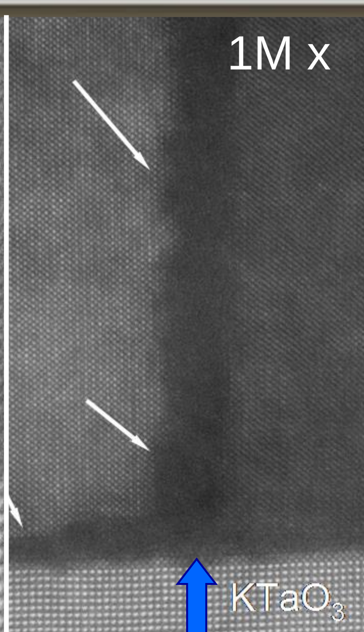

discontinuity of the SLCO film

Interface roughness

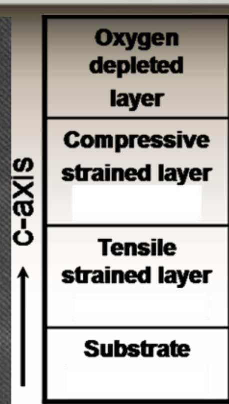

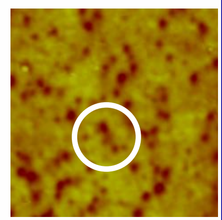

AFM of $KTaO_3$

on (001) $KTaO_3$

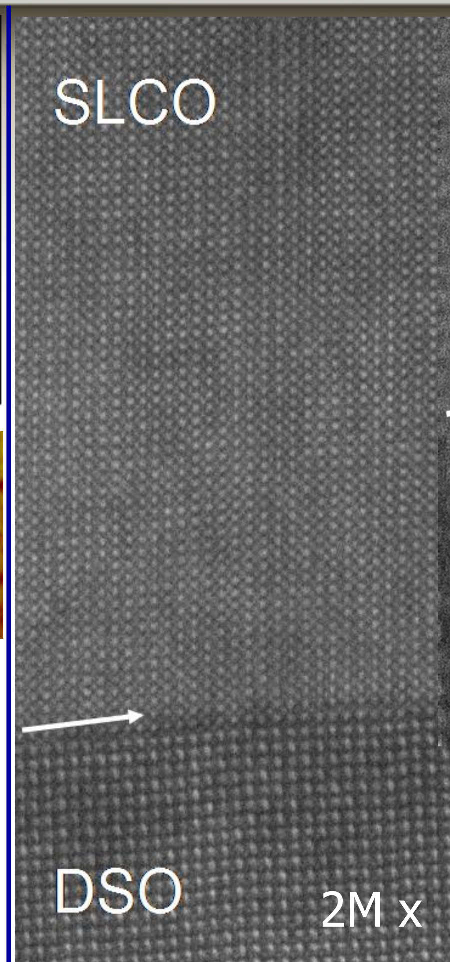

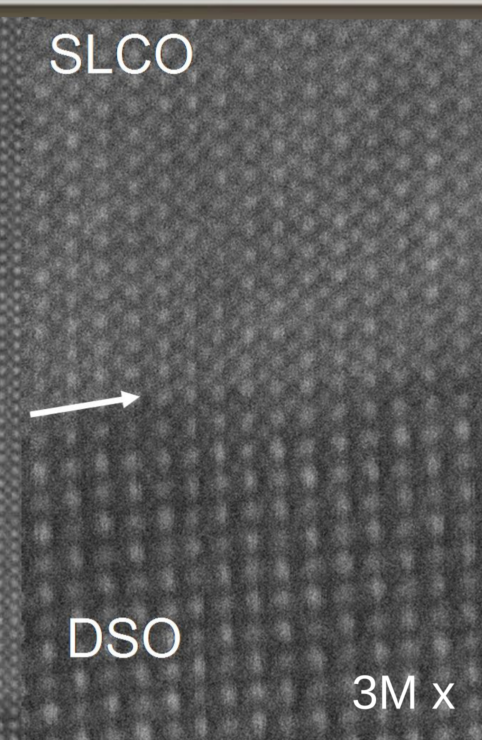

no defects;
sharp interface;
no interface strained layer

on (110) $DyScO_3$

Pairing symmetry from phase sensitive experiments

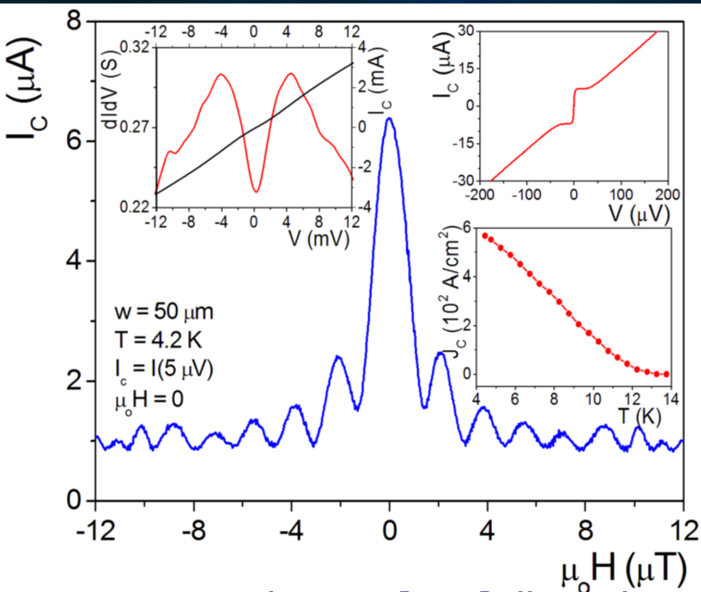

Symmetric 30º, [001] tilt grain boundary SLCO junction data

- No ZBCP observed in GB junctions

Schematic layout of the 0- and π-SQUIDs

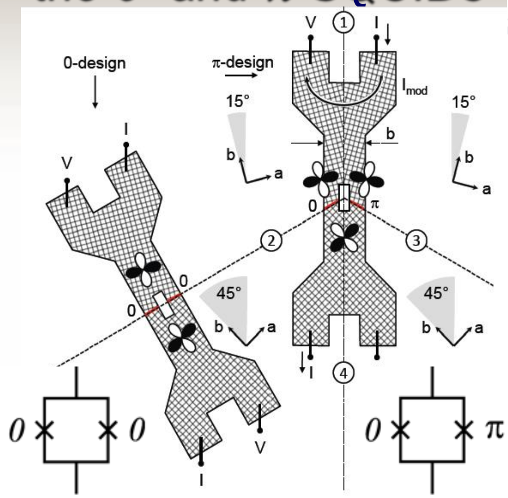

I_c vs magnetic field for a) 0- and b) π-SQUIDs

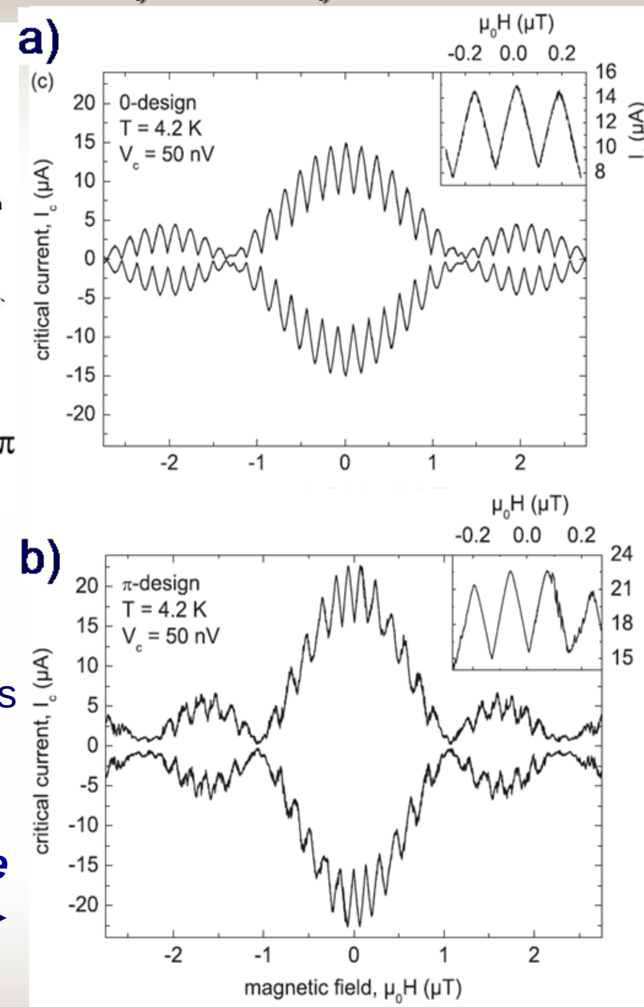

Geometry designed to be frustrated for d-wave pairing;
If d-wave: the dc-SQUID ring around the tetracrystal point contains one 0-junction and one π-junction (forming the π-SQUID, which exhibits an additional π shift in its phase).

The I_c vs. H shows a minimum at H=0 for the π-SQUID due to the phase shift across the π-junction.

Predominantly $d_{x^2-y^2}$ pairing symmetry

Schulz et al., APL 76 (2000); Chesca et al., PRL 90 (2003)

Tomaschko et al., Phys. Rev. B 86 (2012)

Conclusions

- the superconducting properties of the PLD grown electron-doped $Sr_{1-x}La_xCuO_2$ thin films are still far of those of the bulk or of the MBE grown films; however, higher phase stability can be achieved by PLD (in the over doped region);

- epitaxial strain controls the initial growth mechanism and, as a result, the final microstructural (structural defects and oxygen network) and transport properties of the films;

- the films grown on (110) $DyScO_3$ show almost perfect epitaxy; structural defects present in the films grown on $KTaO_3$ help in removing the excess oxygen, these films showing the best superconducting properties;

- no zero bias conductance peak observed in grain-boundary junctions, but phase sensitive experiments shown a predominantly d-wave order parameter symmetry in $Sr_{0.85}La_{0.15}CuO_2$ films.

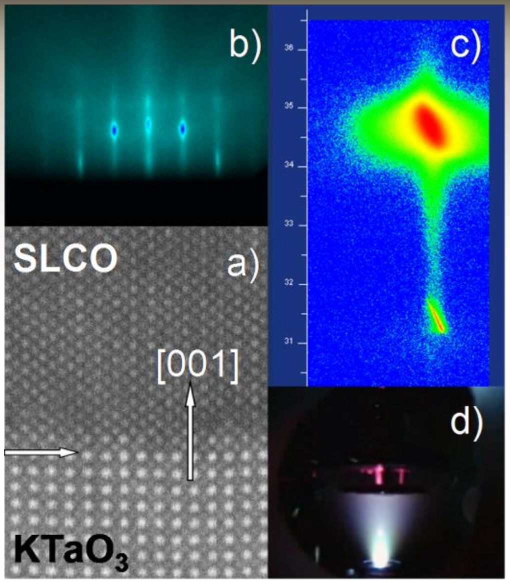

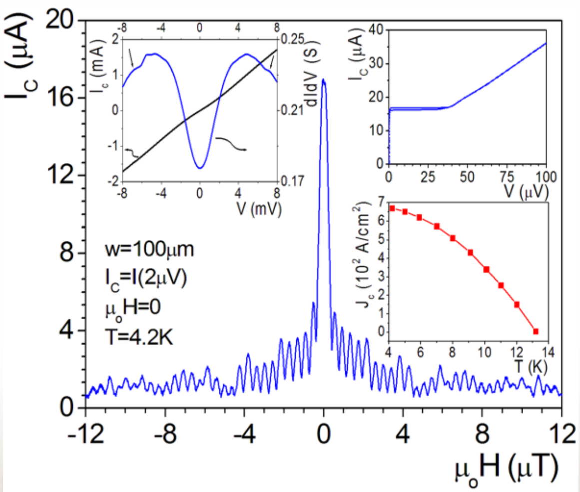

Acknowledgements

Deutsche Forschungsgemeinschaft (project KL 930/11)

Romanian National Authority for Scientific Research, CNCS UEFISCDI, project number PNII-ID-PCE-2011-3-1065

European Commission under the FP7 Capacities programme (EUMINAfab project number 1090)